University of Belgrade, Faculty of Physics

Marina Radulaški

Numerical Simulations of Electron-Phonon Interaction in Quantum Dots

diploma thesis

Belgrade, July 2011

I have been intrigued by the quantum laws of nature ever since I first encountered them as a high school student in Petnica Science Center. My interests broadened and grew through my studies at University of Belgrade Faculty of Physics and internships at the Institute of Physics Belgrade, Polish Academy of Sciences Institute of Physics, Austrian Academy of Sciences Institute for Quantum Optics and Quantum Information, Oxford University, Helmholtz Center Berlin and Lawrence Berkeley National Laboratory. I am grateful to these institutions, as well as to the people I collaborated with, for helping me define and pursue my scientific interests.

I would like to thank my thesis supervisor Dr. Nenad Vukmirović of Scientific Computing Laboratory, Institute of Physics Belgrade, for introducing me to the theories and powerful numerical approaches essential for my thesis research, and for making an invaluable contribution to my academic progress. I would also like to thank Dr. Lin-Wang Wang of Lawrence Berkeley National Laboratory for the opportunity to work on this project and for guiding my development within it.

Finally, I am very grateful to my family and friends who supported me and believed in me throughout this segment of my life and education.

in Belgrade, July 2011 *Marina Radulaški*

Contents

1

Introduction

The ongoing energy crisis, which is only to exasperate by the passage of time, calls for the rapid development of renewable energy sources. At the same time, the alarming emission of greenhouse gases by the conventional sources, motivates the pursuit for greener options. The abundance of solar energy paves a promising path for dealing with these problems.

Among the existing solar technologies, solar cells based on quantum dots are of specific interest [1]. The demonstrated capability of quantum dots to generate multiple electron-hole pairs (*excitons*) out of a single energetic photon may increase the efficiency per cell, while the quantum dots with intermediate band allow for the utilization of photons with energies below the band gap. The study of these solar cells is tightly bound with the investigation of the electronic transport in quantum dots. Therein lies the motivation for the research of this thesis.

1.1 Quantum Dots

Quantum dots are nanostructures whose carriers are confined in all three spatial dimensions. Their properties are in between those of the bulk and the single molecules, and are dependent on the method of their assembly [1].

Electrostatic quantum dots are fabricated by the restriction of the two dimensional electron gas in a semiconductor heterostructure laterally by electrostatic gates, or vertically by etching techniques. The properties of this type of quantum dots, can be controlled by the change of the applied potential at gates, the choice of the geometry of gates or by external magnetic field. The typical size of these dots is of the order of 100 nm. In general, they are not considered practical for mass production.

Self-assembled quantum dots are obtained through the growth of layers on top of each other in heteroepitaxial systems with different lattice constants. This growth mode is called Stranski-Krastanov mode, while the most common experimental techniques of the epitaxial nanostructure growth are Molecular Beam Epitaxy and Metalorganic Chemical Vapor Deposition. Self-assembled quantum dots typically have lateral dimensions of the order of 15 – 30 nm and height of the order 3 – 7 nm. Their high price limits them from the industrial applications.

Colloidal quantum dots or *nanocrystals* are synthesized as single crystals of the size of a few nanometers, using chemical methods. Their size and shape can be controlled by the duration, temperature and ligand molecules used in the synthesis. Colloidal quantum dots are typically of spherical shape with the diameter sometimes as low as 2 – 4 nm. These quantum dots represent a good candidate for solar cell applications, due to their low price as well as favorable electron transport properties in the case when they are interconnected by molecules.

This thesis considers CdSe quantum dots. The crystal structure of CdSe may take two forms – *wurtzite* and *zinc blende* [2], shown in Figure 1.1. Zinc blende is a two-component analog to the diamond structure and is represented as Face Centered Cubic with bases 0 and $\frac{1}{4}(\hat{x}+\hat{y}+\hat{z})$. Wurtzite is a two-component analog of hexagonal diamond structure and is represented by hexagonal lattice with bases 0 and $\frac{1}{3}\hat{a}+\frac{1}{3}\hat{b}+\frac{1}{2}\hat{c}$. In the case of CdSe the parameters of these structures are $a = 0.608$ nm for zinc blende and $a = 0.4135$ nm and $c = 0.6749$ nm for wurtzite.

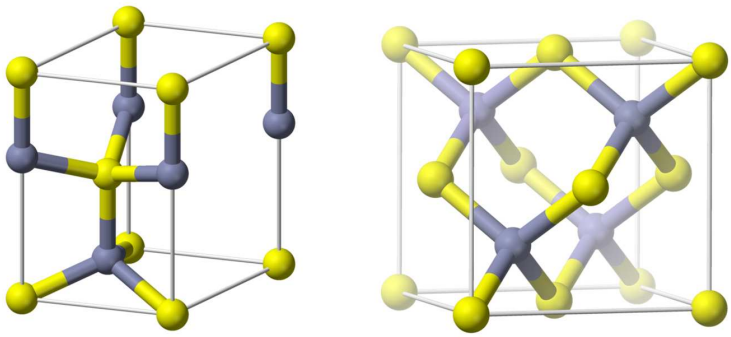

Figure 1.1: Two crystal structures of CdSe: wurtzite (left) and zincblende (right) [3].

Some of quantum dot properties of fundamental interest are the controllable charging with an arbitrary number of electrons and the possibility to be used as a qubit. Aside from the previously mentioned solar cells, the applications of quantum dots span over biological labels, light emitting diodes, lasers, optical amplifiers, single photon sources and photodetectors [1].

1.2 Purpose of the Thesis

This thesis investigates electron-phonon interaction in colloidal CdSe quantum dots. As it will be explained later, electron-phonon interaction takes the lead role in the electron transport between quantum dots, which is one of the most important aspects of quantum dot solar cells. The choice of the material is irrelevant from the principal point of view, since the conclusions can be generalized onto other materials. CdSe represents a good option to work with because its properties have been investigated thoroughly and there is enough experimental data available to check the validity of the derived results.

2

Theory

A typical quantum dot examined in this thesis contains several thousand valence electrons. To gain any hope of calculating electron energy levels and wave functions one has to switch to a single-particle picture of an electron in the effective potential originating from its interactions with other electrons. In order to do this, we employ the Density Functional Theory and a method derived from it, the Charge Patching method, which speeds up the process by avoiding the self-consistent calculations. Using the energies and wave functions calculated this way, we proceed to electron-phonon interaction calculations. In the end we apply Marcus Theory to calculate transition rate[1] between two quantum dots. The following sections describe all the steps in detail.

2.1 Density Functional Theory

Density Functional Theory (DFT) [4, 5], developed in 1964 and 1965 by Pierre Hohenberg[2], Walter Kohn[3] and Lu Jeu Sham[4] makes it possible to map the interacting many-electron system onto a system of noninteracting electrons moving in an effective potential due to all the other electrons. This is given by Kohn-Sham equations that read [5, 6]

$$(-\frac{1}{2}\nabla^2 + V_{ion} + V_H + V_{XC})\psi_i(\mathbf{r}) = \epsilon_i\psi_i(\mathbf{r}) \tag{2.1}$$

$\psi_i(\mathbf{r})$ and ϵ_i are the wave functions and energies of so-called *Kohn-Sham orbitals* and $V_{ion}(\mathbf{r})$ is the potential of all nuclei in the system. Hartree potential $V_H(\mathbf{r})$ is given as[5]

$$V_H(\mathbf{r}) = \int d\mathbf{r}' \frac{\rho(\mathbf{r}')}{|\mathbf{r} - \mathbf{r}'|}, \qquad \rho(\mathbf{r}) = \sum |\psi_i(\mathbf{r})|^2 \tag{2.2}$$

where ρ represents the electronic charge density of the system, and its summation goes over all occupied Kohn-Sham orbitals. The exchange correlation potential V_{XC} in (2.1) accounts for all other effects of electron-electron interactions beyond the simple Coulomb repulsion, but since its form is unknown this potential has to be approximated. The most

[1] Transition rate represents probability for transition per unit time.

[2] Pierre Hohenberg (born 1934), French-American theoretical physicist.

[3] Walter Kohn (born 1923), Austrian-born American theoretical physicist, Nobel Prize in Chemistry in 1998.

[4] Lu Jeu Sham, Chinese-American theoretical physicist.

[5] The system of atomic units where the reduced Planck's constant $\hbar$, the electron mass m_0 and the electron charge e are all equal to 1 is used.

common approximation is Local Density Approximation (LDA) [5] which assumes the dependence on local electronic charge only. If the electron density at a point $\mathbf{r}$ is $n(\mathbf{r})$, the exchange-correlation energy per electron $\epsilon_{XC}(\mathbf{r})$ is calculated as in the case of the free electron gas of the same density. The value of the LDA exchange-correlation potential is given as $V_{XC}(\mathbf{r}) = \frac{\delta E_{XC}[n(\mathbf{r})]}{\delta n(\mathbf{r})}$, where $E_{XC}[n(\mathbf{r})] = \int \epsilon_{XC}^{free}(\mathbf{r}) n(\mathbf{r}) d^3\mathbf{r}$.

Kohn-Sham and charge density equations have to be solved self-consistently, so that the occupied electronic states generate charge density which produces the electronic potential that is used to construct the equations. This makes DFT calculations computationally demanding. Another downside of this approach is that one has to calculate all the orbitals ψ_i in each iteration, which is redundant for most applications where only a few states around the gap are needed. An alternative approach that avoids the full self-consistent calculations without loss in accuracy is presented in the next section.

2.2 Charge Patching Method

Trying to avoid the lengthy self-consistent calculations in charge density calculations Lin-Wang Wang[6] developed the Charge Patching method (CPM) in 2002 [7]. The main assumption of this method is that the charge density around an atom depends only on its local atomic surrounding. This is justified if there is no long range external electric field to cause long-range charge transfer, e.g.when there is a band gap in the material. The idea of this method is to calculate the charge density of a small prototype system and decompose it into contributions from individual atoms called *charge density motifs*. While approaching a large system, these motifs can be patched together to give the total charge density. Charge density motifs are calculated as

$$m_{I_\alpha}(\mathbf{r} - \mathbf{R}_\alpha) = \rho_{prototype}(\mathbf{r}) \frac{\omega_\alpha(|\mathbf{r} - \mathbf{R}_\alpha|)}{\sum_{\mathbf{R}_{\alpha'}} \omega_{\alpha'}(|\mathbf{r} - \mathbf{R}_{\alpha'}|)} \tag{2.3}$$

where $\mathbf{R}_\alpha$ is the position of atom type α, $m_{I_\alpha}(\mathbf{r}-\mathbf{R}_\alpha)$ is the charge density motif of this atom type, while I_α stands for its atomic environment; $\omega_\alpha(r)$ is an exponentially decaying function that defines the partition function $\frac{\omega_\alpha(|\mathbf{r}-\mathbf{R}_\alpha|)}{\sum_{\mathbf{R}_{\alpha'}} \omega_{\alpha'}(|\mathbf{r}-\mathbf{R}_{\alpha'}|)}$ which divides space into overlapping regions of each atom, thus making $m_{I_\alpha}(\mathbf{r} - \mathbf{R}_\alpha)$ a localized function that can be stored in a fixed size numerical array. Upon obtaining the motifs one can calculate the total charge density of the large nanosystem by summing over each atom's assigned motifs

$$\rho_{patch}(\mathbf{r}) = \sum_{\mathbf{R}_\alpha} m_{I_\alpha}(\mathbf{r} - \mathbf{R}_\alpha). \tag{2.4}$$

After constructing the whole charge density one can proceed to calculate Hartree potential by solving Poisson's[7] equation $\triangle V = -\frac{\rho}{\epsilon}$ and, along with LDA formula for exchange-correlation potential, obtain the single particle Hamiltonian.

The Charge Patching method was tested for carbon fullerenes, semiconductor alloys, semiconductor impurities, organic molecules and polymers and semiconductor quantum dots.

[6] Lin-Wang Wang, Chinese-American theoretical physicist.

[7] Siméon Denis Poisson (1781-1840), French mathematician, geometer and physicist.

The generated patched charge densities are typically within 1% of the self-consistently calculated LDA charge densities, and the corresponding energies are within 30 meV. Typical numerical uncertainty (due to basis function truncations and different nonlocal pseudopotential treatments) of LDA calculations is about the same order of magnitude. Therefore, the Charge Patching method can be considered as accurate as the direct *ab initio*[8] calculations for these systems.

2.3 Passivation

When dealing with the colloidal quantum dots, special care has to be taken about their surface. The surface of the bare crystal consists of dangling bonds that introduce band gap states. One of the ways to remove band gap states is so-called *passivation* which implies pairing of the dangling bond electrons with other electrons [1]. Since every atom inside the quantum dot has four neighbors, if it has m valence electrons, it contributes with $m/4$ electrons per bond, while its neighbors provide $2-m/4$ electrons each, forming the eight-electron configuration in the highest occupied orbital. Same way, each dangling bond provides $m/4$ electrons and needs to be passivated by $2-m/4$ electrons. To keep the system locally neutral there also has to be a positive $2-m/4$ nuclear charge. The simplest passivation agent is therefore a hydrogenlike atom with $2-m/4$ of both electrons and positive nuclear charge Z. For IV-IV group materials like Si, $Z=1$ and one is dealing with the hydrogen atom, while for II-VI systems, Z has a noninteger value and such atoms are called *pseudohydrogen* atoms. These artificial pseudohydrogen atoms do describe the essential features of good passivation agents and serve as simplified models for the real passivation situations, where organic molecules with complicated and often unknown structure are involved.

2.4 Transport Mechanisms

To achieve better electron transport, quantum dots are often connected by a molecule as shown in Figure 2.1. This assures that the wave functions overlap.

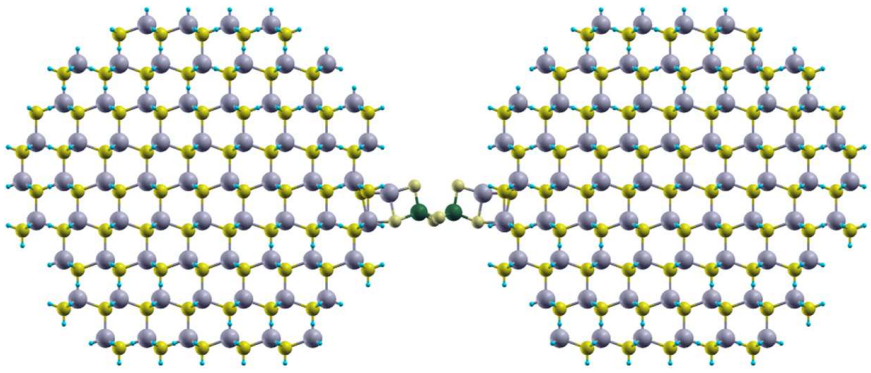

Figure 2.1: Two quantum dots connected by a linker molecule.

[8]Latin term meaning "from the beginning".

There are different possible mechanisms for electron transport between quantum dots connected by a molecule [8]:

(a) a narrow bulk band formed by the coupling of nearby quantum dot wave functions and a bulk crystal like Bloch state electron transport;

(b) the tunneling mechanism where the electron transports from one quantum dot to a nearby quantum dot purely by electronic coupling without the help of the phonon;

(c) over-the-barrier activation mechanism, where electrons are thermally excited to quantum dot eigenstates with energies higher than the potential barrier at the linker, then they transport freely to the other side of the barrier;

(d) the phonon assisted hopping, where the electron hops from one dot to a nearby dot by absorbing one or multiple phonons.

All these scenarios are schematically depicted in Figure 2.2. Theoretically speaking, without material-specific, quantitative calculations, all the above mechanisms are possible. The quantitative calculations are therefore critical for providing qualitative insights to the mechanism of the transport. However, in the case of quantum dots considered here, it will be shown that phonon assisted hopping gives the main contribution.

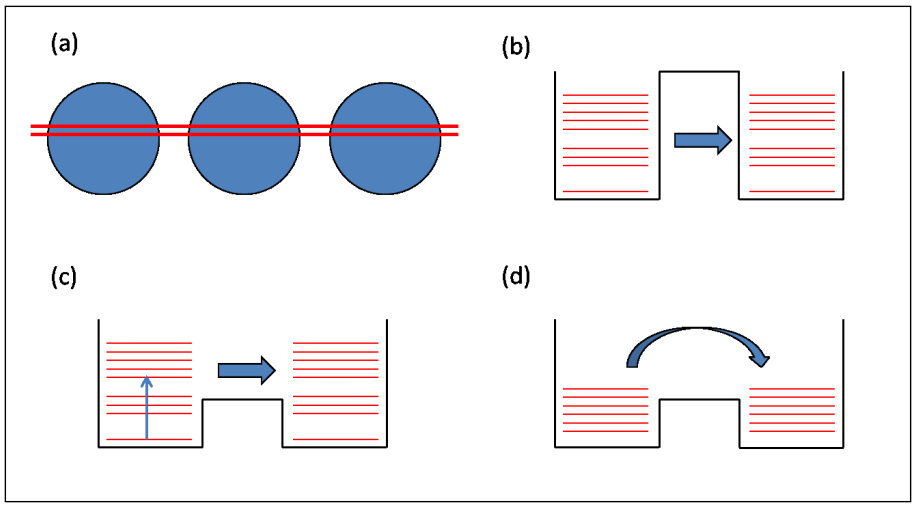

Figure 2.2: Possible mechanisms for electron transport between two quantum dots connected by a molecule. (a) bulk crystal like Bloch state electron transport; (b) direct tunneling mechanism without the help of phonon; (c) over-the-barrier activation mechanism and (d) phonon assisted hopping.

2.5 Electron-Phonon Interaction

Phonon is a quasiparticle arising from the quantization of the vibrational energy in a crystal. The eigenenergies and eigenvectors of phonon modes are obtained by the diagonalization of the dynamical matrix defined as

$$K_{rs,pq} = \frac{1}{\sqrt{m_r m_p}} \frac{\partial^2 E}{\partial x_{rs} \partial x_{pq}} \tag{2.5}$$

where E is the total energy of the system, m_r is the mass of the r-th atom and x_{rs} is its s-th coordinate ($s \in 1, 2, 3$) [1]. Each eigenvalue is a squared angular frequency ω_μ of a phonon mode μ

$$\sum_{pq} K_{rs,pq} R_{pq}^{(\mu)} = \omega_\mu^2 R_{rs}^{(\mu)} \tag{2.6}$$

and the normal coordinate of mode μ is given as

$$\nu_\mu = \sum_{rs} R_{rs}^{(\mu)} (x_{rs} - x_{rs}^0) \sqrt{m_r} \tag{2.7}$$

where $(x_{rs} - x_{rs}^0)$ represents the s-th coordinate displacement of atom r from its equilibrium position.

Inside a quantum dot electrons are interacting with phonons making transitions between electronic states. The Hamiltonian of this interaction is given as

$$H_{e-ph} = \sum_{i,j,\mu} \mathcal{M}_{i,j,\mu} a_i^\dagger a_j (b_\mu + b_\mu^\dagger) \tag{2.8}$$

where $a_{i/j}, a_{i/j}^\dagger, b_\mu, b_\mu^\dagger$ are the annihilation and creation operators for electrons and phonons respectively, $\mathcal{M}_{i,f,\mu} = \langle \psi_i | \frac{\partial H_0}{\partial \nu_\mu} | \psi_f \rangle$ is the electron-phonon coupling matrix element between electronic states i and f, with H_0 being the single particle Hamiltonian $H_0 = -\frac{1}{2}\nabla^2 + V_{ion} + V_H + V_{XC}$.

To calculate the change $\frac{\partial H_0}{\partial \nu_\mu}$ one can displace each atomic coordinate by a small Δx_{rs} in the direction s to obtain $\frac{\partial H_0}{\partial x_{rs}}$, and then use (2.7) to perform a transformation. The Charge Patching method is particularly suitable to efficiently compute the displacements $\frac{\partial H_0}{\partial x_\mu}$ since the only difference in the charge density between the perturbed and equilibrium configurations comes from the charge density motifs of the displaced atom and its neighbors.

2.6 Marcus Theory

Studying electron transport in chemical reactions, Rudolph Marcus[9] developed in 1956 a theory [9] about electron transfer rate between two chemical species shown in Figure 2.3. The initial and final states are vibrational levels of molecules (or in our case quantum dots) and the transfer rate is given by the Fermi[10] Golden Rule as

$$k_{CT} = \frac{2\pi}{\hbar^2} |V|^2 \sum_\nu \sum_{\nu'} P_{i\nu} |\langle \Theta_{f\nu'} | \Theta_{i\nu} \rangle|^2 \delta(\omega_{f\nu',i\nu}) \tag{2.9}$$

where V is the electronic coupling between initial and final states, $\Theta_{i/f}$ are the nuclear (ionic) vibration wave functions of the initial/final states, consisting of product of independent harmonic oscillators $\Theta_{i/f,\nu} = \prod_j \chi_{i/f,\nu_j}(Q_j)$, $P_{i\nu}$ is the distribution function for the collection of quanta ν_j of the initial state and $\omega_{f\nu',i\nu}$ is the energy difference between final state with

[9] Rudolph Marcus (born 1923), Canadian chemist, Nobel Prize in Chemistry in 1992.
[10] Enrico Fermi (1901-1954), Italian-American physicist, Nobel Prize in Physics in 1938.

vibrational quantum numer ν' and initial state with vibrational quantum number ν. After some derivation [10], equation (2.9) can be expressed as

$$k_{CT} = \frac{1}{\hbar^2}|V|^2 \int_{-\infty}^{\infty} dt \, \exp\{i\omega_{fi}t - \sum_j S_j[(2\bar{n}_j + 1) - \bar{n}_j e^{-i\omega_j t} - (\bar{n}_j + 1)e^{i\omega_j t}]\} \qquad (2.10)$$

where $\omega_{fi} = \frac{\Delta G}{\hbar}$ is the difference between the equilibrium energies of initial and final state divided by $\hbar$, $\bar{n}_j = \frac{1}{e^{\hbar\omega_j/k_bT}-1}$ denotes the population of the jth normal mode and ω_j is its frequency, $S_j = \frac{\lambda_j}{\hbar\omega_j}$ is the Huang-Rhys factor measuring the electron-phonon coupling strength and can be also expressed through electron-phonon coupling matrix element as $S_j = \frac{|\langle\psi_i|\frac{\partial H}{\partial \nu_j}|\psi_i\rangle|^2}{\omega_j^2}$, while λ_j is the contribution of the jth mode to the reorganization energy. In the case of the strong coupling $\sum_j S_j \gg 1$ and high-temperature limits (2.10) gets the form of *Marcus formula*

$$k_{CT} = \frac{|V|^2}{\hbar}\sqrt{\frac{\pi}{\lambda k_B T}} \exp(-\frac{(\lambda + \Delta G)^2}{4\lambda k_B T}) \qquad (2.11)$$

with $\lambda = \sum_j \lambda_j$. In this formula the nuclear (ionic) vibrational effect is accounted for classically.

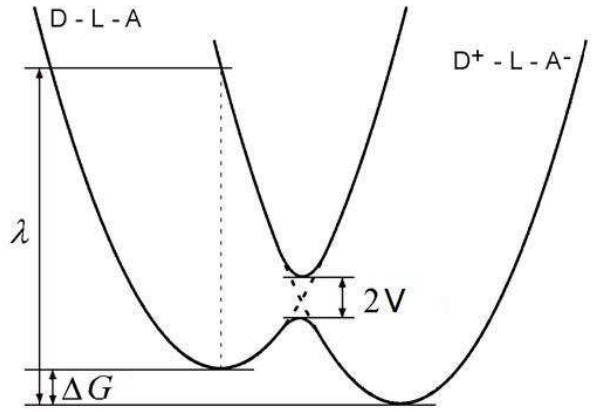

Figure 2.3: Energy scheme in Marcus theory transfer calculations [3].

3

Simulation

Numerical modeling of quantum dot systems investigated in this thesis was based on the theory presented in the previous chapter. The electronic structure was calculated by the Charge Patching method and used as input to determine the electron-phonon coupling.

All computational codes used were written in FORTRAN programming language and were executed on National Energy Research Scientific Computing Center's Franklin Cray XT4 parallel processing system with 38.128 Opteron computer cores and a peak performance of 352 TFlops/sec [11]. The calculations used around 200.000 processor hours.

3.1 Electronic Structure

To calculate the electronic structure we start with the generation of quantum dot crystal structure with the geometry described at Figure 1.1. The complexity of this algorithm is linear in the number of atoms N. Using the Charge Patching method we patch motifs illustrated in Figure 3.1 onto corresponding parts of the crystal structure to construct the charge density. This process is also linear in N.

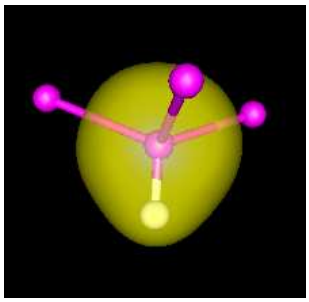

Figure 3.1: An example of a charge density motif at the edge of a quantum dot. Purple dots are Cd and Se atoms, white dot is a pseudohydrogen atom and yellow surface represents sample charge density isosurface.

Using Fourier transform to solve Poisson's equation with the calculated charge density, we obtain the potential created by electronic charge distribution in O($NlogN$) complexity. Having determined the electronic potential, we solve Kohn-Sham equations by the Folded Spectrum Method [12] which, instead of Hamiltonian H, uses $(H - E_{ref})^2$, where E_{ref} is reference energy, and solves the equations by the Conjugate Gradient Method [13]. These

two operators have same eigenstates and this change allows for the calculation of an arbitrary number of states around E_{ref} instead of the calculation of all states from ground energy on, which is convenient because we are interested only in the energy states around the band gap. The complexity of this step is O($LNlogN$), where L is the number of levels desired. Notice that the complexity of this whole calculation is at most O(N^2logN), and for most applications just O($NlogN$), while the standard DFT approach scales as O(N^3). This introduces a significant speed up to calculations of large quantum dots.

Analyzing the degeneracies and the shape of the states in the conduction band, one can notice the energy levels are formed similarly as orbitals in an atom. The examples of calculated conduction band states are given in Figure 3.2. The bandgap dependence on the quantum dot diameter is given in Figure 3.3 and shows that the energy needed to excite an electron over the bandgap increases as the size of the quantum dot decreases. We fitted this dependence to a power law and obtained the results in agreement with experimental data for CdSe [14].

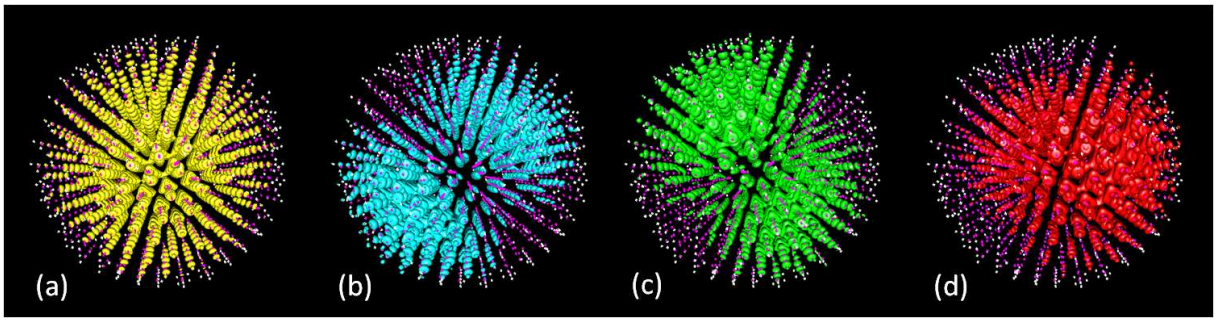

Figure 3.2: First four conduction band states in a zinc blende 2047-atom CdSe quantum dot calculated by the Charge Patching method. Purple dots are Cd and Se atoms, white dots are pseudohydrogen atoms. (a) represents s-state with energy 0.918 eV, while the other states are degenerate p-states with energies (b) 1.251 eV (c) 1.253 eV (d) 1.258 eV. The value of the fifth conduction band energy is 1.567 eV.

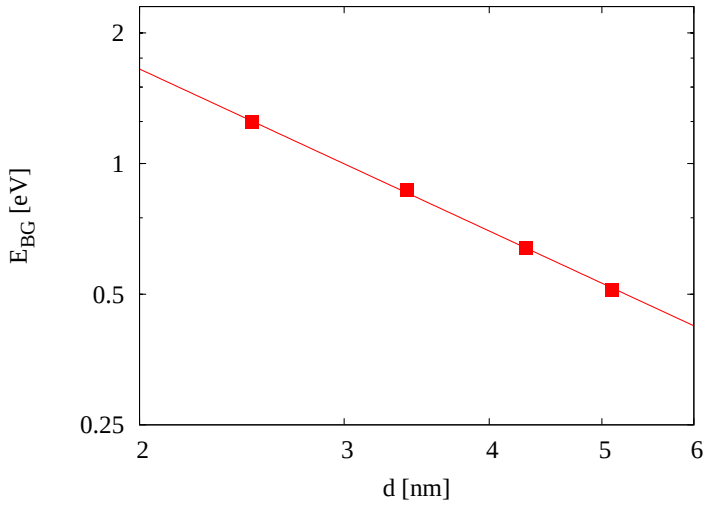

Figure 3.3: The bangap size dependence on the diameter of colloidal wurtzite CdSe quantum dot and its fit to $E_{BG} = cd^{-\alpha}$, $c = 3.9(2)$, $\alpha = 1.24(3)$.

To check the correctness of the method used we compared DFT and Charge Patching calculations on a 465-atom zinc blende quantum dot and noticed the spectra are displaced by 0.14 eV, but have the same value of the band gap 2.03 eV and the same splitting between the first two conduction band levels 0.56 eV. Therefore, we conclude that the Charge Patching method gives the correct spectrum for the purposes of this research.

3.2 Electron-Phonon Coupling

The goal of our simulation was to calculate matrix elements $\langle\psi_{CBM}|\frac{\partial H_0}{\partial x_{ks}}|\psi_{CBM}\rangle$ in quantum dots of various sizes. These results can be used in research studying electron-phonon interaction in quantum dots.

We start with the generation of crystal structures in which a single atom (r-th atom) is displaced in x, y or z-direction (s-th direction) for a displacement which is small compared to the inter-ionic distance, in our case $\Delta x_{rs} = 0.01$ Å. This is done for each Cd and Se atom and each direction with the complexity $\mathrm{O}(N^2)$. Then, as described in the previous section, we patch charge densities and solve Poisson's equation to get the potential V_{rs}^{el}. Subtracting the non-displaced potential from V_{rs}^{el} we obtain their difference ΔV_{rs}^{el} in $\mathrm{O}(N^2)$ time.

To check the correctness of the obtained potential difference we compared it to the one calculated by DFT and found a certain mismatch. This is due to the fact that the Charge Patching method (in the current version) accounts only for changes in the charge density around the displaced atom and its neighbors. Therefore it does not properly take into account the screening of the field of the charge density induced by the atomic displacement. For proper consideration of such screening, one would also have to take care of the changes in charge density of atoms further away from the displaced atom. To correct this mismatch, we constructed *mask function* to scale Charge Patching electron potential difference in the neighborhood of the displacement to the value of DFT electron potential difference. The mask function has an exponential form

$$w(\mathbf{r}) = \mathbf{b} + \mathbf{e}^{-\frac{(\mathbf{r}-\mathbf{r_{atom}})^2}{\mathbf{r_b^2 a^2}}} \tag{3.1}$$

where $\mathbf{r_{atom}}$ is the coordinate of the atom being displaced (before the displacement), $r_b = 0.529$ Å is Bohr radius, while a and b are constant parameters which take values $a = 4.0$, $b = 0.2$ for Cd atom and $a = 2.5$, $b = 0.0$ for Se atom, Figure 3.4. Multiplying the change of electron potential difference obtained by the Charge Patching method we get a good estimate of the exact value of electron potential difference. This fix was calculated using results for 465-atom zinc blende CdSe quantum dot, and can be used for other dot sizes, as well as for the wurtzite structure. It executes in $\mathrm{O}(N^2)$ time.

Having corrected the electron potential difference and including ionic potential difference we proceed to calculate $\langle\psi_i|\Delta V_{rs}|\psi_j\rangle$ for first 20 non-displaced conduction band states $\psi_{i/j}$ and displacements of each atom (r-th atom) in each direction (s-th direction). The complexity of this step is $\mathrm{O}(N^2)$. Dividing calculated values by Δx_{rs} we obtain $\mathcal{C}_{rs}^{(ij)} = \langle\psi_i|\frac{\partial V}{\partial x_{rs}}|\psi_j\rangle$. To justify the correctness of the mask function we compare these values to those calculated by DFT method for several atoms r. We find good agreement within 30% error which is illustrated in Figure 3.5.

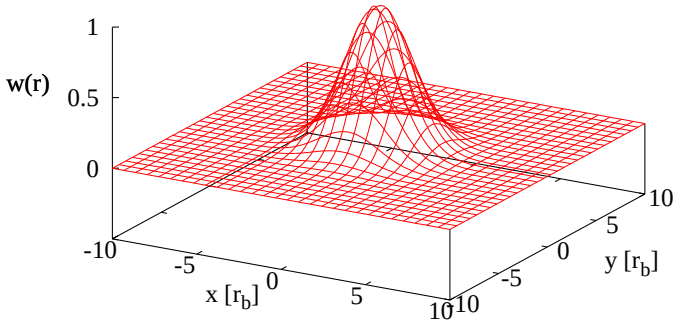

Figure 3.4: The shape of the mask function $w(\mathbf{r}) = \mathbf{e}^{-(\mathbf{r}-\mathbf{r_{atom}})^2/(\mathbf{2.5r_b})^2}$ for scaling the potential difference around an Se atom, shown in $x-y$ plane for $z=0$, $r_b = 0.529$ Å.

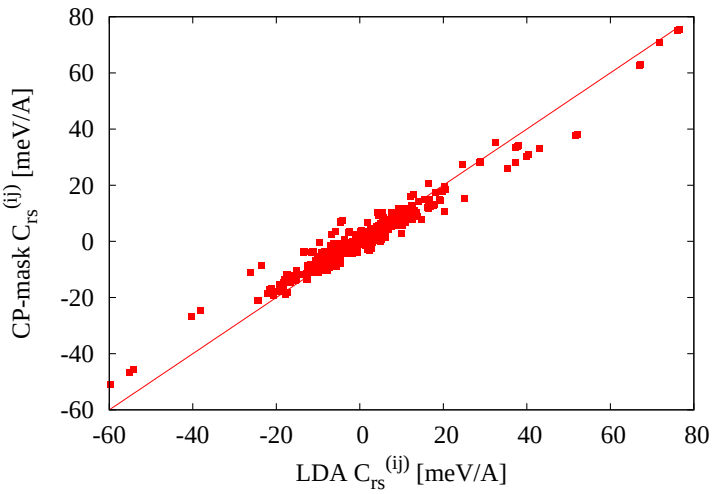

Figure 3.5: Comparison between real part of $\mathcal{C}_{rs}^{(ij)}$ values calculated by the Charge Patching method with mask function and DFT approach for a sample atom r in a 465-atom zinc blende CdSe quantum dot. The $y = x$ line is given as a reference.

Finally, using the non-displaced conduction band minimum (CBM) states we calculate (also in $O(N^3)$ time) $\mathcal{C}_{rs} = \langle\psi_{CBM}|\frac{\partial H_0}{\partial x_{rs}}|\psi_{CBM}\rangle = \langle\psi_{CBM}|\frac{\partial V}{\partial x_{rs}}|\psi_{CBM}\rangle$. Figure 3.6 shows the dependence of $\mathcal{C}_{rs}$ values along quantum dot diameter in x-direction for displacement along the $s = x$ direction for different sizes of the quantum dot.

The dependences shown in Figure 3.6 show the same trend for all dot sizes and change the sign as they cross the center of the dot. This can be explained through the following theoretical reasoning. The potential change $\frac{\partial V}{\partial x_{rs}}$ can be reasonably approximated with the delta function derivative. Then

$$\mathcal{C}_{rs} \sim \int |\psi_{CBM}|^2 \delta'(x - x_{atom}) dx = -\frac{d}{dx}|\psi_{CBM}|^2\Big|_{x=x_{atom}}. \tag{3.2}$$

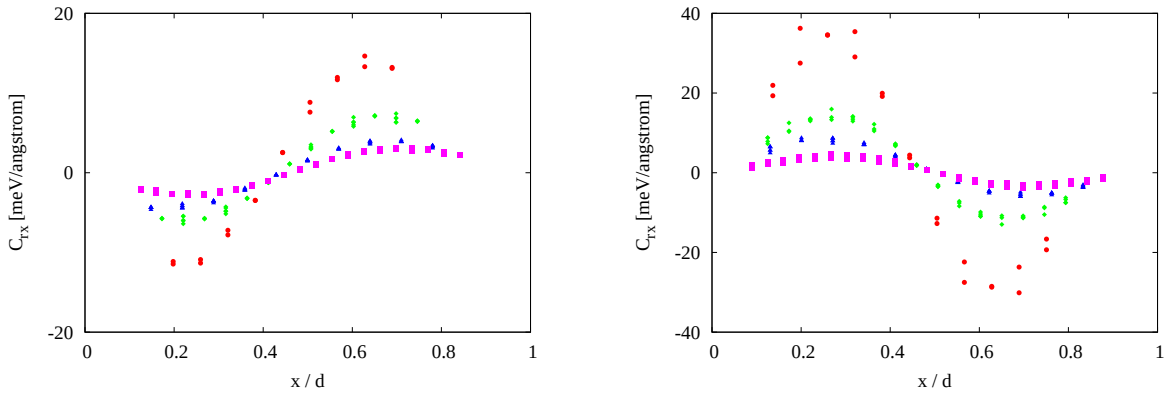

Figure 3.6: Dependence of $\mathcal{C}_{rs}$ values for Cd atoms (left) and Se atoms (right) along diameter (in relative coordinates) in x-direction for the displacements in $s = x$ direction for wurtzite CdSe quantum dot. Red dots denote quantum dot of 468 atoms and $d = 2.5$ nm diameter, green diamonds: 1051 atoms and $d = 3.4$ nm, blue triangles: 1916 atoms and $d = 4.3$ nm, magenta squares: 3193 atoms and $d = 5.1$ nm.

CBM state is an s-state which is totally symmetric and, watching along x-direction, $|\psi_{CBM}|^2$ is a Bell curve. Its derivative is positive in the first half of the diameter, zero in the center of the quantum dot, and negative in the second half of the diameter, which explains why $\mathcal{C}_{rs}$ changes the sign in the center of the dot. The absolute value of $\mathcal{C}_{rs}$ gets bigger as the dot gets smaller. This is due to the increase of $|\psi_{CBM}|^2$ when the dot diameter decreases, as a consequence of normalization of ψ_{CBM}. Finally, the inverse dependence of Cd compared to Se comes from the the fact that the charge densities around their ions have opposite signs, since their oxidation states are Cd^{+2} and Se^{-2}.

In the next chapter we will show how the obtained results can be used for investigation of electron transport between quantum dots.

4

Applications

The results presented in the previous chapter were applied in the research of electron transport in quantum dots connected by a molecule, done in Lawrence Berkeley National Laboratory, Berkeley, California [15], in the group of Dr. Lin-Wang Wang. Relaxation energy was calculated using the obtained values of $\mathcal{C}_{rs}$, electronic coupling was calculated separately and these two were combined in Marcus Theory for the calculations of electron transport [8].

4.1 Molecular Attachment

Experiments have shown that colloidal quantum dots can form periodic crystal structures, *supercrystals*, interconnecting themselves with different linker molecules. Such quantum dot supercrystals have unique mechanical, thermal, electrical and optical properties and the experiments have studied these aspects. However, there has not been much support from theoretical calculations to explain their electron transport mechanisms.

One of the synthesized supercrystals which showed strong conductivity is made of CdSe quantum dots connected by Sn_2S_6 molecule [16, 17]. It represents a suitable material to model the transport mechanisms on. In order to study the electron conductivity one can first study electron transport between two quantum dots connected by a linker molecule and perform *ab initio* calculations. A typical quantum dot in experiments is ∼5 nm in diameter and consists of ∼3.000 atoms. This means the two-dot system has ∼6.000 atoms which is beyond the limit of current computational power if DFT method is used. However, the Charge Patching method described in previous chapters can be successfully applied with a minor loss in accuracy.

The investigation of the molecule-quantum dot attachment starts with the study of the attachment between the Sn_2S_6 molecule and a flat CdSe $(10\bar{1}0)$ surface. Two types of attachment shown in Figure 4.1 were studied [8]. Type I has two end S atoms connected to two neighboring Cd atoms, one in plane, one standing out of the plane. Type II has Sn-S_2-Sn rhombus rotated for 90 degrees and its two end S atoms attached to a standout Cd and another two Cd atoms in plane. The standout Cd atom is used to satisfy the local electron counting rule. Type II attachment has closer distance between the molecule and the surface, and is 0.5 eV more stable.

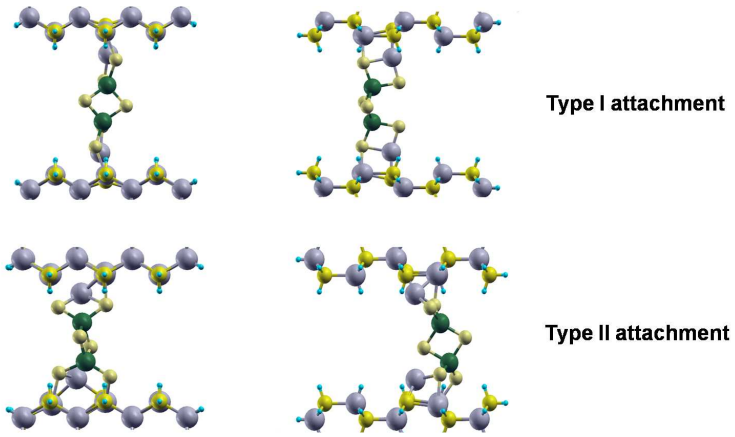

Figure 4.1: Type I and type II attachment of Sn_2S_6 to flat CdSe $(10\bar{1}0)$ surface [8].

4.2 Electronic Coupling

To calculate the charge density, the system is divided into three parts: two quantum dots and a molecule attached to small parts of quantum dots. The latter consists of ∼500 atoms passivated with pseudohydrogens and can be calculated self-consistently using DFT. For two quantum dots the Charge Patching method was used, as described in Section 3.1. Gathering the charge densities from all three parts and solving Poisson's equation one gets electron potential needed to solve the DFT single particle equation (2.1). Once conduction band energy levels are determined [8], one can notice that the first two states are very close and represent electron localized in one or the other quantum dot Figure 4.2a.

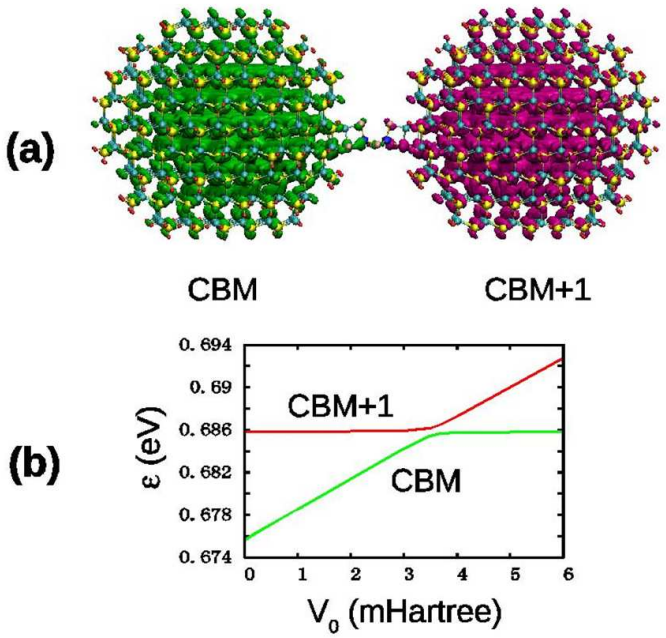

Figure 4.2: (a) Isosurfaces of the charge densities of CBM (green, left) and CBM+1 (purple, right) electron states. (b) The eigenenergies for CBM and CBM+1 as functions of the added small external potential at one quantum dot, in the case of 1916-atom CdSe wurtzite quantum dots, type I attachment [8].

The main step of charge transport is electron transfer from one quantum dot state to another quantum dot state. The electronic coupling of these two states can be calculated by their anticrossing which is done by artificially adding a small external potential at one quantum dot and driving the energy of its eigenstate over the energy of the other eigenstate. This is shown in Figure 4.2b and the anticrossing is twice the value of electron coupling V_c. As the quantum dot size gets smaller the value of V_c gets larger. This dependence is given in Figure 4.3 for both types of attachments [8].

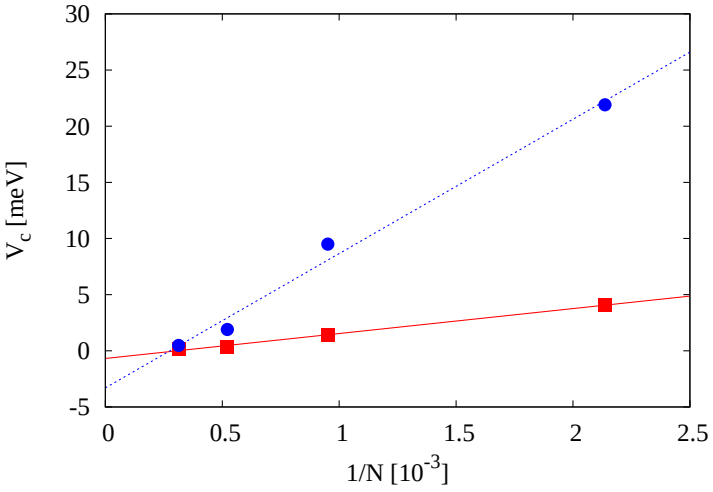

Figure 4.3: Electron coupling dependence on inverse number of atoms and the corresponding linear fit, for colloidal CdSe quantum dots connected by Sn_2S_6 molecule [8]. Values for type I attachment are shown in red squares, while type II attachment is shown in blue circles.

4.3 Reorganization Energy

Since the linker molecule has small phonon density of states, and the wave function from Figure 4.2a has very small amplitude at the molecule, the phonon modes from the molecule can be ignored and electron-phonon coupling can be restricted to electron-phonon coupling within each quantum dot.

The matrix elements $\mathcal{C}_{rs}$ obtained in Section 3.2 were used to calculate electron-phonon coupling matrix $\mathcal{M}_{i,j,\mu}$ whose diagonal elements are needed to determine the reorganization energy λ, as theoretically described in Section 2.6. The dependence of relaxation energy on inverse number of atoms in quantum dot is given in Figure 4.4.

4.4 Charge Transfer Rate

Using the calculated electron coupling and relaxation energy, the charge transfer rate $k_{CT} = \tau^{-1}$ can be calculated with Marcus formula (2.11). This approach treats the phonon degree of freedom classically and does not allow quantum tunneling of the atomic movement. The inclusion of the quantum mechanical treatment gives the formula (2.10). In both approaches τ^{-1} is a function of equilibrium energy difference between the dots $\Delta G = \epsilon_a - \epsilon_b$ which is

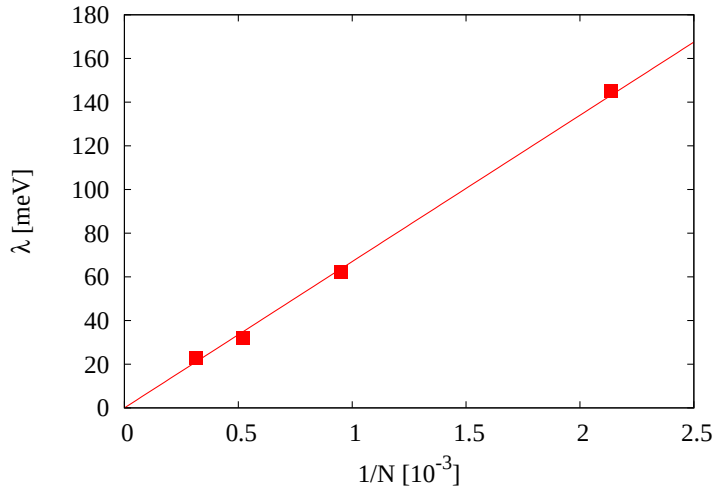

Figure 4.4: Relaxation energy dependence on inverse number of atoms in a colloidal CdSe quantum dot with the corresponding linear fit [8].

zero in case of equal quantum dots.

In order to model a more realistic case one should allow for fluctuation in size of quantum dots and consequently in the value of $\epsilon_a - \epsilon_b$. Figure 4.5 compares the values of hopping rates for Marcus formula and quantum treatment for different sizes of quantum dots [8]. One can see a remarkable agreement of the two approaches around $\epsilon_a - \epsilon_b = 0$.

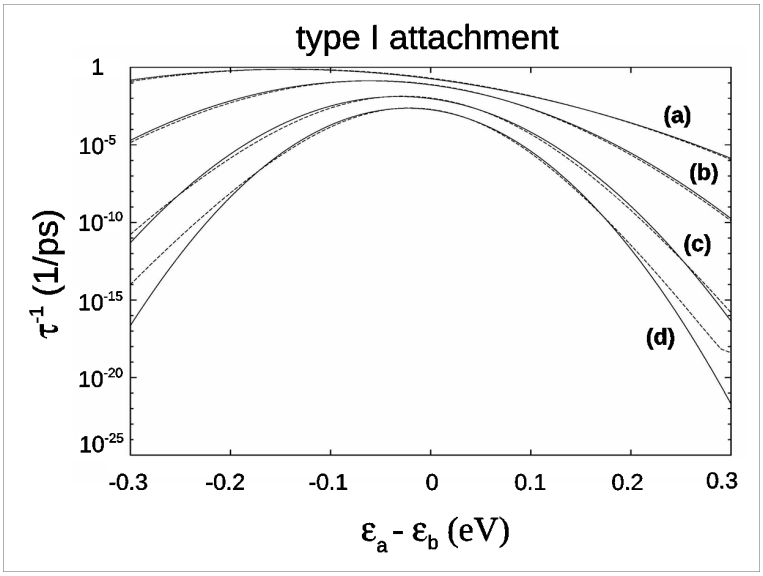

Figure 4.5: The electron hopping rate dependence on the eigenenergy difference between the two quantum dots at room temperature for the cases of (a) 468-atom quantum dot, (b) 1051-atom, (c) 1916-atom and (d) 3193-atom, type I molecular attachment [8]. Solid curves represent the Marcus theory result, while the dashed curves represent quantum phonon treatment.

4.5 Electron Transport Mechanism

From the results of performed calculations one can get insight into the nature of electron transfer between quantum dots. Out of the transport mechanisms presented in Section 2.4 phonon-assisted hopping emerges as dominant [8]:

(a) Since the reorganization energies 4.4 are much bigger than the electron coupling 4.3, the electrons prefer to be localized in a single quantum dot to gain the reorganization energy instead of being in an extended state to gain the electron coupling energy. Therefore, the mini-band picture (Fig 2.2a) will not hold.

(b) For direct tunneling to work without the involvement of phonons, the other side should have a continuous density of states to conserve the energy, but this is not the case, since the other quantum dot has discrete energy levels above CBM. The possibility of resonant tunneling should also be neglected. For resonant tunneling to occur, the eigenenergy difference $\epsilon_a - \epsilon_b$ should be within the coupling constant V_c. Typically there is 5% size fluctuation between the quantum dots which corresponds to 50 meV change in eigenenergy for experimentally relevant 5.1 nm diameter quantum dot. This is a hundred times bigger than V_c, therefore no direct tunneling without phonons (Fig 2.2b) is possible.

(c) In direct hopping over the barrier (Fig 2.2c) the electron can jump to a level above the potential barrier, due to thermal fluctuations. In the case of $d = 5.1$ nm the barrier is about $E_b = 2.4$ eV. The estimated hopping rate is $\tau_0^{-1} e^{-E_b/k_B T} \sim 10^{-39}$ ps^{-1}. This is much smaller then the multi-phonon hopping rate described by Marcus theory, and can therefore be ignored.

(d) The multi-phonon assisted process (Fig 2.2d) described by Marcus theory proves to be the most likely charge transfer mechanism between the two quantum dots.

4.6 Carrier Mobility

To check the agreement of this approach with the experiment, one can compare the values of the carrier mobility in a quantum dot supercrystal [18]. The dot size in the chosen experiment [17] is 4.5 nm with 5% size fluctuation and its mobility is $\mu = 3 \cdot 10^{-2}$ cm^2/V/s. The closest of the four dots considered is the one with 4.3 nm diameter. Three cases are considered: no size fluctuation, 5% size fluctuation, and 5% size fluctuation with a uniform distribution of $|V_c|^2$ between zero and values given in Figure 4.3. The last uncertainty comes from the assumption that the quantum dot-molecule attachment is not as good as described by either type I or type II and that there are some loose attachments. The calculated mobility values are given in Table 4.1.

The 5% size fluctuation decreases the value of mobility by a factor 1.7, and the loose attachment further reduces it by a factor 5 [8]. The results for type I attachment agree very well with the experimental result, while type II attachment is an order of magnitude larger. Therefore, one can conclude that majority of the attachments is type I-like. Also, the model in which pairs of quantum dots are interconnected by a single Sn_2S_6 molecule agrees quite well with the experiment.

5% size fluctuation	uniform connection fluctuation	μ_I [cm^2/V/s]	μ_{II} [cm^2/V/s]
No	No	8.22×10^{-2}	2.16
Yes	No	4.80×10^{-2}	1.26
Yes	Yes	1.02×10^{-2}	0.26

Table 4.1: The mobility μ for type I and type II molecule attachment in a quantum dot supercrystal with $d = 4.3$ nm. The experimental value for the case of 4.5 nm-quantum dot array is $3 \cdot 10^{-2}$ cm^2/V/s [8].

5

Conclusions

This thesis models electron-phonon interaction in non-organic quantum dots on the example of colloidal CdSe quantum dots.

Using the Charge Patching method it has been shown how to accurately calculate electronic structure for large quantum dots (∼3.000 atoms) which are beyond the reach of Density Functional Theory self-consistent calculations, with the currently available computational resources.

For the calculations of electron-phonon interaction in quantum dots, an approximation of *mask function* has been developed to scale the results of electron potential for crystal structures with a displaced atom, obtained by the Charge Patching method, to agree with the exact Density Functional Theory results. This approximation makes it possible to calculate matrix elements $\mathcal{C}_{rs} = \langle \psi_{CBM} | \frac{\partial H_0}{\partial x_{rs}} | \psi_{CBM} \rangle$ for large quantum dots, which are needed in calculations of electron-phonon coupling matrix.

The values of $\mathcal{C}_{rs}$ have been calculated for four different quantum dot sizes. The dependence of these values along the quantum dot diameter has been analyzed and its trend has been theoretically derived.

The applications of the obtained results in the research of CdSe quantum dot supercrystals connected by Sn_2S_6 linker molecule by two types of attachment in Dr. Lin-Wang Wang's group at Lawrence Berkeley National Laboratory have been presented. The electron transfer rate has been calculated for multi-phonon assisted hopping and this has been proved to be the dominant mechanism of charge transport in such supercrystals. The mobility for both types of attachment has been calculated and the results have shown close agreement with the experimental values.

References

[1] N. Vukmirovic, L-W. Wang, Comprehensive Nanoscience and Technology **1**, 189 (2011).

[2] `http://www.nrl.navy.mil/`

[3] `http://www.wikipedia.org/`

[4] P. Hohenberg, W. Kohn, Phys. Rev. **136**, B864 (1964)

[5] W. Kohn, L.J. Sham, Phys. Rev. **140** A1133 (1965)

[6] M.C. Payne, M.P. Teter, D.C. Allan, T.A. Arias, J.D. Joannopoulos, Rev. Mod. Phys. **64**, 4 (1992).

[7] L-W. Wang, Phys. Rev. B **65**, 153410 (2002)

[8] I.H. Chu, M. Radulaski, N. Vukmirovic, H.P. Cheng, L-W. Wang, Charge transport in a quantum dot supercrystal, submitted

[9] R.A. Marcus, Rev. Mod. Phys. **65**, 3 (1993).

[10] G. Nan, X. Yang, L. Wang, Z. Shuai, Y. Zhao, Phys. Rev. B **79**, 115203 (2009)

[11] `http://www.nersc.gov/`

[12] L-W. Wang, A.J. Zunger, J. Chem. Phys. **100**, 2394 (1993)

[13] M.P. Teter, M.C. Payne, D.C. Allan, Phys. Rev. B **40**, 12255 (1989)

[14] C.B. Murray, D.J. Norris, M.G. Bawendi J. Am. Chem. Soc. **115** 8706 (1993)

[15] `http://www.lbl.gov/`

[16] D. V. Talapin, J. S. L., M. V. Kovalenko and E. V. Shevchenko. Chem. Rev. 2010, 110, 389–458.

[17] M.V. Kovalenko, M. Scheele, D.V. Talapin, Science **324**, 1417 (2009)

[18] N. Vukmirovic, L-W. Wang, Nano Lett. **9** 3996 (2009)